COMMUNICATION

Check for updates

Single crystal MnOOH nanotubes for selective oxidative coupling of anilines to aromatic azo compounds†

Yong Zou,[a] Mingkai Zhang,[a] Fangxian Cao,[a] Jiayuan Li,[b] Sai Zhang (iD) *[b] and Yongquan Qu*[ab]

Catalytic synthesis of aromatic azo compounds by oxidative coupling of anilines using molecular oxygen represents a facile, green and valuable process; however, such an economical process suffers from poor catalytic activity and selectivity. Herein, novel single crystal MnOOH nanotubes with abundant Mn^{3+} sites and high oxygen defects were successfully synthesized. The catalyst exhibited high selectivity for oxidative coupling of anilines, achieving complete transformation into aromatic azo compounds under mild conditions, even at room temperature.

Introduction

Aromatic azo compounds, as important chemicals and intermediates, are widely used as dyes, pigments, food additives, drugs and precursors for functional materials.[1–5] Traditionally, these compounds are prepared by oxidative coupling of anilines using a stoichiometric amount of nitrite salts and/or toxic oxidants and processed *via* diazonium, which is less atom-economic, yielding stoichiometric inorganic salts as solid wastes.[6–8] In contrast, the catalytic synthesis of aromatic azo compounds from aniline derivatives by using O_2 as the oxidant represents a much more sustainable process. Afterwards, various heterogeneous catalysts including metal oxides (*e.g.* RuO_2/Cu_2O), supported metals (*e.g.* Au/TiO_2, Au/CeO_2, Ru/Al_2O_3, Ag) and metal–organic frameworks (*e.g.* Cu-BTC) delivered the capability for the oxidative coupling of aromatic anilines to aromatic azo compounds.[1,9–15] Despite these impressive advances achieved, in general, harsh reaction

[a]Frontier Institute of Science and Technology, Xi'an Jiaotong University, Xi'an, 710049, China

[b]Key Laboratory of Special Functional and Smart Polymer Materials of Ministry of Industry and Information Technology, School of Chemistry and Chemical Engineering, Northwestern Polytechnical University, Xi'an 710072, China. E-mail: zhangsai1112@nwpu.edu.cn; yongquan@nwpu.edu.cn

conditions and even sacrificial additives are required to guarantee successful oxidative coupling (Table S1†). In addition, the chemoselectivity towards azo products and catalytic recyclability are unsatisfactory, which significantly restrict the practical applications of the existing catalytic systems. Thus, the search for cost-effective and efficient catalysts with high selectivity to synthesize aromatic azo compounds under mild conditions is greatly significant in both fundamental studies and industrial production.[16–19]

Mn-based nanomaterials as environmentally friendly and cheap transition metal catalysts exhibit great potential in various oxidation reactions.[20–24] For the oxidative coupling of aromatic anilines, the Mn^{3+} centre of MnO_x is generally considered as the catalytically active site *via* the formation of radical intermediates along with the transfer of electrons to Mn^{3+}.[1,25] However, it is still a great challenge to achieve the oxidative coupling reaction for Mn-based catalysts as well as other non-precious metal-based catalytic systems in the absence of additives under mild conditions. Previous reports have revealed that toluene as solvent can significantly promote the catalytic activity of oxidative coupling reactions. However, it is still an irreconcilable contradiction between high catalytic activity and the high selectivity of aromatic azo compounds due to the easily generated by-product between anilines and benzaldehydes oxidized from toluene.[25] Therefore, achieving the simultaneous improvement of catalytic activity and selectivity and understanding the mechanism at the molecular level are of great significance for the oxidative coupling of aromatic anilines to aromatic azo compounds.

Along this line, the most stable manganese oxyhydroxide (also known as γ-MnOOH) with abundant Mn^{3+} may exhibit satisfactory performance in catalytic oxidative coupling of anilines to aromatic azo compounds, which hasn't been explored yet. Meanwhile, one-dimensional (1D) nanostructures have gained attention in various heterogeneous oxidation reactions due to the high possibility of tailoring the surface physicochemical properties of catalysts by tuning their defects, sizes and compositions.[26–31] Herein, single crystal MnOOH

nanotubes (NT-MnOOH) were successfully synthesized, delivering high selectivity for the oxidative coupling of anilines to aromatic azo compounds even in toluene at room temperature under 0.5 MPa O_2, in comparison with the low activity of MnOOH nanowires (NW-MnOOH) and Mn_2O_3. The detailed characterization studies suggest that the controllable surface hydroxyl proportions of MnOOH result in the modulation of surface Mn^{3+} fractions and the concentration of surface oxygen defects. Mechanistic investigations reveal that the abundant Mn^{3+} sites and rich surface oxygen defects of NT-MnOOH are identified as the key factors (1) to effectively activate the adsorbed oxygen and generate active oxidative species and (2) to enable the strong adsorption of anilines and sequential activation, resulting in greatly enhanced catalytic activity and selectivity.

Preparation and characterization of catalysts

The NT-MnOOH and NW-MnOOH catalysts were prepared by a hydrothermal method, as described in the Experimental section (ESI†). The typical nanotube and nanowire morphology features could be obtained by controlling the hydrothermal reaction times and the concentrations of the precursors. As shown in Fig. 1a, the X-ray diffraction (XRD) patterns of NT-MnOOH and NW-MnOOH revealed the monoclinic structure of γ-MnOOH (JCPDS 41-1379). The tube-like morphology of NT-MnOOH with average inner and outer diameters of 8.0 ± 1.7 nm and 27.7 ± 5 nm (Fig. S1†), respectively, was confirmed from the transmission electron microscopy (TEM) image (Fig. 1b) and the energy dispersive spectroscopy (EDS) mapping (Fig. S2a†). The high-resolution TEM (HRTEM) image displayed the distinct lattice fringes of 0.223 nm and 0.328 nm, corresponding well to the (2,1,0) and (−1,1,1) planes of γ-MnOOH, respectively

(Fig. 1c). The nanowire structure of NW-MnOOH with an average diameter of 43.6 ± 27 nm was also revealed from the TEM image (Fig. 1d and S3†). The lattice fringe of 0.330 nm matched well with that of the (−1,1,1) plane of γ-MnOOH (Fig. 1e).

Catalytic performance

The oxidative coupling of aniline was selected as the model reaction to explore the catalytic performance of NT-MnOOH and MW-MnOOH. The NT-MnOOH catalyst successfully realized the selective transformation of aniline into an aromatic azo compound, which was optimized in toluene under 0.5 MPa O_2 at 25 °C (Table S2†). As shown in Fig. 2a, 88.0% conversion of aniline was achieved after 44 h. Importantly, only 1,2-diphenyldiazene was yielded, indicating high selectivity towards aromatic azo compounds. Under the optimized reaction conditions, no oxidative coupling of aniline occurred in the absence of catalysts (Table S2†), which indicated the natural catalytic capability of NT-MnOOH. However, the NW-MnOOH catalyst exhibited low catalytic activity for the oxidative coupling of aniline. The benchmark catalyst of Au nanoparticles supported on TiO_2 (Au/TiO_2, Fig. S5†), synthesized according to a previous report,[1] also delivered no oxidative coupling product at 25 °C (entry 14). The oxidative coupling of aniline also did not occur in the presence of Mn_2O_3 (as a typical manganese oxide, Fig. S4†) or MnOOH nanosheets (NS-MnOOH, as a typical manganese oxyhydroxide nanosheet, Fig. S4†), as shown in Fig. 2a. Therefore, these comparative experiments demonstrated the intrinsic catalytic nature of NT-MnOOH for the selective oxidative coupling of aniline to an aromatic azo compound at room temperature.
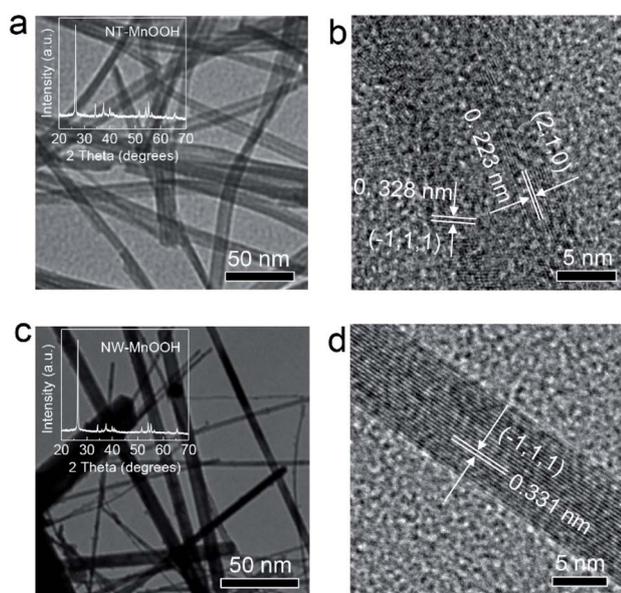
Fig. 1 (a) TEM and (b) HRTEM images of NT-MnOOH. Inset in (a) is the XRD pattern of NT-MnOOH. (c) TEM and (d) HRTEM images of NW-MnOOH. Inset in (c) is the XRD pattern of NW-MnOOH.
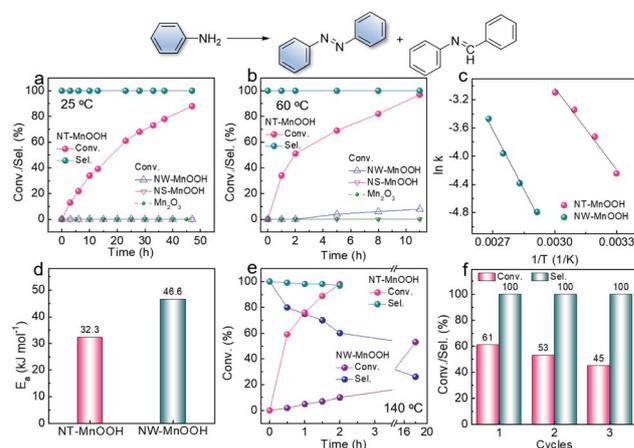
Fig. 2 Catalytic performance of oxidative coupling of aniline to an aromatic azo compound at (a) 25 °C and (b) 60 °C, respectively. Reaction conditions: aniline (0.5 mmol), catalyst (20 mg), toluene (2 mL) and 0.5 MPa O_2. (c) Plot of ln k vs. $1/T$ for NT-MnOOH and NW-MnOOH, derived from reaction rates vs. time. (d) E_a of NT-MnOOH and NW-MnOOH. (e) Catalytic performance of oxidative coupling of aniline to an aromatic azo compound at 140 °C. Reaction conditions: aniline (0.5 mmol), catalyst (20 mg), toluene (2 mL) and 0.5 MPa O_2. (f) Recyclability of NT-MnOOH. Reaction conditions: aniline (0.5 mmol), NT-MnOOH (20 mg), toluene (2 mL), 25 °C, 0.5 MPa O_2 and 24 h.

This journal is © The Royal Society of Chemistry 2021

J. Mater. Chem. A, 2021, **9**, 19692–19697 | **19693**

When the reaction temperature was raised to 60 °C, enhanced activity of NT-MnOOH was observed, reaching 97% conversion of aniline after 11 h (Fig. 2b). Most importantly, the catalytic selectivity towards azobenzene was well preserved. In contrast, Mn_2O_3 and NS-MnOOH still exhibited no catalytic activity; while only 8% conversion was realized by NW-MnOOH under identical conditions (Fig. 2b). Even normalizing to specific surface areas (Fig. S6†), the catalytic activity of NT-MnOOH was still greatly higher than that of NW-MnOOH as well as the MnOOH with other morphologies.

To further explore the intrinsic catalytic activity of NT-MnOOH, kinetic experiments were performed. As shown in Fig. S7 and S8,† the concentrations of aniline decreased almost linearly with time at each temperature, revealing near zero order reaction characteristics. Thus, the oxidative coupling of aniline was not limited by the external diffusion of reactants. The apparent activation energies (E_a) can be derived from the Arrhenius equation (Fig. S9, S10† and 2c). As shown in Fig. 2d, the much lower E_a of NT-MnOOH (32.3 kJ mol^{-1}) in comparison with that of NW-MnOOH (46.6 kJ mol^{-1}) suggested the higher intrinsic activity of NT-MnOOH for the oxidative coupling of aniline.

Toluene was optimized as the best solvent for the oxidative coupling of aniline herein (Table S2, entries 1–6†). However, the oxidation of toluene to benzaldehyde and the consequent condensation between benzaldehyde and aniline to N-benzylideneaniline could significantly reduce the chemoselectivity towards azo compounds.[1,25] To our delight, herein, the NT-MnOOH catalyst not only delivered the highest catalytic activity, but also exhibited >99.9% selectivity of 1,2-diphenyldiazene at both 25 °C and 60 °C (Fig. 2a and b). The yield of by-product N-benzylideneaniline was below the detection limit of GC. When the reaction temperature was further raised to 140 °C, the complete transformation of aniline was accomplished within 2 h. Importantly, the selectivity of azobenzene still reached as high as 97% (Fig. 2e). At such a high reaction temperature of 140 °C, the NW-MnOOH catalyst yielded a 53% conversion of aniline after 16 h. However, the selectivity of azobenzene was only 26% associated with a 74% selectivity of N-benzylideneaniline as the by-product (Fig. 2e). Therefore, the NT-MnOOH catalyst exhibited simultaneously enhanced catalytic activity and selectivity for the oxidative coupling of aniline to azobenzene.

The catalytic stability of NT-MnOOH is also a very important criterion to evaluate its catalytic performance. After the reaction, NT-MnOOH can be easily separated by centrifugation and washed with excess toluene and acetonitrile several times for the next cycles. The oxidative coupling of aniline was performed at 24 h and 25 °C. Although the conversion of aniline decreased from 61% to 45% from the first cycle to the third cycle, selectivity of 1,2-diphenyldiazene was impressively preserved (>99%, Fig. 2f). Also, the unchanged morphology and phase of the spent NT-MnOOH demonstrated its satisfactory catalytic and structural stability (Fig. S11†).

Catalytic mechanism

Next, the catalytic mechanism was explored to understand the catalytic activity and selectivity of NT-MnOOH under such mild reaction conditions. In the previous mechanism studies for the oxidative coupling of aniline to 1,2-diphenyldiazene,[1,25] the first step is recognized as a single-electron oxidation of aniline to the radical cation via electron transfer from aniline to an interfacial metal centre. Afterwards, azobenzene is formed after the successive loss of protons and electrons from the corresponding intermediates. Herein, the oxidation of aniline was completely blocked when 2,6-di-tert-butyl-4-methylphenol (0.6 mmol) as a trapping agent was added to consume the aniline radical cation, suggesting a similar reaction pathway (Fig. S12†). The corresponding coupling product between 2,6-di-tert-butyl-4-methylphenol and the aniline radical cation was detected by GC and GC-MS (Fig. S13†). Thus, this control experiment proved that the formation of the aniline radical cation was the critical step in the oxidative coupling of aniline. Generally, the generation of the aniline radical cation should accompany the reduction of surface active Mn^{3+} to Mn^{2+}, along with the release of the labile lattice oxygen. Therefore, the surface Mn^{3+} level of MnOOH is demonstrated as the key factor herein.

Then, the surface properties of the two catalysts were analyzed by XPS. As shown in Fig. 3a, the binding energy of Mn 2p revealed a higher Mn valence state of NT-MnOOH than that of NW-MnOOH, which could be attributed to the weaker reducibility due to the shorter hydrothermal time. The average oxidation state (AOS) of Mn can be calculated from the binding energy of Mn 3s doublet peaks using $AOS = 8.956 - 1.126 \times \Delta E$.[32,33] The ΔE values for NT-MnOOH and NW-MnOOH, derived from the Mn 3s peaks, were 5.23 and 5.40 eV, respectively (Fig. 3b). Thus, the AOS values of Mn were determined to be 3.06 and 2.86 for NT-MnOOH and NW-MnOOH, respectively. When the AOS value of catalysts is larger than 3.0, it indicates the presence of high valent Mn^{n+} species ($n > 3.0$). However, an AOS value below 3.0 suggests the co-existence of low valent Mn^{n+} species ($n < 3.0$) in catalysts. Thus, the absolute value of ΔAOS ($|\Delta AOS|$, defined as $|AOS - 3.0|$) can directly index the abundance of the surface Mn^{3+} species. Apparently, the NT-MnOOH catalyst with a smaller $|\Delta AOS|$ of 0.06 possessed more surface Mn^{3+} species, benefiting the formation of
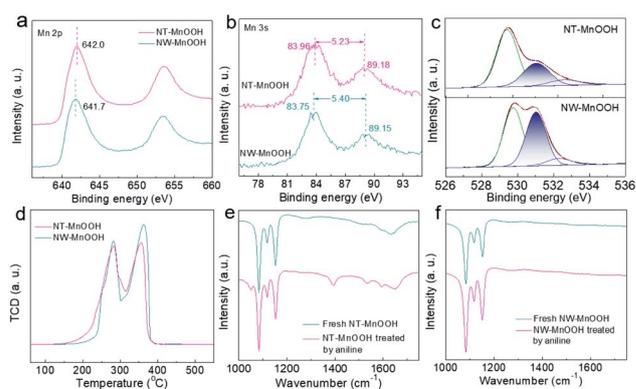
Fig. 3 XPS spectra of (a) Mn $2p_{3/2}$ and (b) Mn 3s for NT-MnOOH and NW-MnOOH. (c) XPS O 1s spectra of NT-MnOOH and NW-MnOOH. (d) H_2-TPR profiles of NT-MnOOH and NW-MnOOH. FT-IR spectra of (e) NT-MnOOH and (f) NW-MnOOH before and after aniline treatment.

19694 | J. Mater. Chem. A, 2021, 9, 19692–19697

This journal is © The Royal Society of Chemistry 2021

the aniline radical cation, compared with NW-MnOOH with a larger $|\Delta AOS|$ of 0.14.

Since the formation of the radical cation is accompanied by the release of the labile lattice oxygen, the strong mobility of lattice oxygen of the catalyst is believed to promote their catalytic activity for the oxidative coupling. Generally, the ideal γ-MnOOH has equal quantities of O^{2-} (Mn–O) and OH^- (Mn–OH). Thus, the ratio of O^{2-}/OH^- derived from the XPS O 1s spectra of MnOOH catalysts can reveal the surface level of oxygen defects. The peaks at binding energies of 529.8, 531.0 and 532.5 eV could be assigned to O^{2-}, OH^- and surface adsorbed oxygen species, respectively (Fig. 3c). The value of O^{2-}/OH^- of NW-MnOOH was 1.05, close to the ideal crystallinity of MnOOH. Comparatively, a much larger O^{2-}/OH^- ratio (2.06) of NT-MnOOH indicated a significantly higher level of oxygen defects. The surface defects result in the loose linkage of Mn–O bonds, which is beneficial to the high mobility of lattice oxygen.[34,35] Also, on evaluation by the H_2-TPR test (Fig. 3d), the relatively lower starting reduction temperature of NT-MnOOH further revealed its stronger mobility of lattice oxygen than that of NW-MnOOH. Thus, it's reasonable to propose the high level of oxygen defects and large amount of Mn^{3+} species in NT-MnOOH as the key factors for the improved catalytic activity of the oxidative coupling of anilines.

In addition, the enhanced selectivity of 1,2-diphenyldiazene for NT-MnOOH was attributed to the competitive adsorption of aniline on catalyst surfaces, which was examined by FT-IR. Compared with the as-prepared NT-MnOOH, two typical peaks at 1280 and 1521 cm^{-1}, which could be respectively assigned to the characteristic vibrations of C–N and C=C, appeared for the aniline-treated NT-MnOOH, suggesting the strong adsorption of aniline on NT-MnOOH (Fig. 3e). In contrast, the FT-IR profiles of NW-MnOOH before and after the aniline-treatments exhibited few changes (Fig. 3f). Consequently, NT-MnOOH with a high level of Mn^{3+} promotes its interaction with anilines instead of solvent toluene owing to the strong electron-donating nature of the amino group, thereby benefiting the activation and subsequent catalysis as well as suppressing the oxidation of toluene to benzaldehyde.

Thus, the competitive adsorption of aniline on NT-MnOOH avoided the generation of N-benzylideneaniline as the by-product and yielded a >99.9% selectivity of 1,2-diphenyldiazene (Fig. 2a). Impressively, such strong aniline adsorption also effectively preserved the selectivity of 1,2-diphenyldiazene over 97% at an even much higher temperature of 140 °C (Fig. 2e). In contrast, NW-MnOOH only yielded a 26% selectivity of 1,2-diphenyldiazene at 58% conversion of aniline after 18 h. The 74% selectivity of N-benzylideneaniline indicated the severe side reaction of toluene oxidation. Therefore, the many surface Mn^{3+} sites on NT-MnOOH resulted in strong aniline adsorption, effectively avoiding the toluene oxidation and thereby enhancing the catalytic selectivity.

Identification of the functions of Mn^{3+} and oxygen defects

In order to further examine the critical roles of the surface Mn^{3+} species and oxygen defects in catalytic activity and selectivity,

a series of NT-MnOOH-t catalysts (t represents the synthetic time) with tailorable surface properties were prepared with prolonged synthetic times under the same conditions. The obtained NT-MnOOH-t catalysts exhibited the typical nanotube morphological features (Fig. S14a–e†) and monoclinic phase of γ-MnOOH (Fig. S14f†). Analysis of their XPS profiles revealed that the binding energy of Mn 2p progressively decreased from 642.0 eV of NT-MnOOH-8 to 641.6 eV of NT-MnOOH-12, along with the AOS values of Mn gradually reduced from 3.06 to 2.83 (Fig. S15†). The values of $|\Delta AOS|$ for various catalysts were also employed as a descriptor to reflect the correlation between catalytic activity/selectivity and the fractions of Mn^{3+} in various NT-MnOOH-t catalysts. The similar values of $|\Delta AOS|$ for NT-MnOOH-8 (0.067), NT-MnOOH-9 (0.048) and NT-MnOOH-10 (0.057), derived from their XPS profiles, suggested the close surface proportions of Mn^{3+} species, while the NT-MnOOH-11 and NT-MnOOH-12 catalysts exhibited a lower Mn^{3+} fraction owing to the much higher $|\Delta AOS|$ values of 0.113 and 0.17, respectively. Meanwhile, as shown in Fig. S16,† the decreased values of the O^{2-}/OH^- ratios revealed the richness of surface oxygen defects for the five catalysts in the order of NT-MnOOH-8 (1.42) > NT-MnOOH-9 (1.28) > NT-MnOOH-10 (1.15) > NT-MnOOH-11 (1.10) > NT-MnOOH-12 (1.09). It is to be noted that when the preparation time was further prolonged to 12 h, the level of the surface defect oxygen of the as-synthesized catalysts tended to a constant by comparing the O^{2-}/OH^- ratios of NT-MnOOH-11 (1.10) and NT-MnOOH-12 (1.09). Therefore, these NT-MnOOH-t catalysts provide an unambiguous platform to investigate the effects of Mn^{3+} and surface oxygen defects on the oxidation coupling of anilines.

The catalytic activity of various NT-MnOOH-t catalysts was characterized by the conversion of aniline as functions of the interfacial Mn^{3+} levels indexed by $|\Delta AOS|$ and the surface oxygen defect abundance described by O^{2-}/OH^- ratios. As shown in Fig. 4a, except for the NT-MnOOH-8 catalyst, the catalytic activity of oxidation coupling of aniline almost linearly decreased with the increase of the $|\Delta AOS|$ values for NT-MnOOH-t catalysts. In particular, with a similar surface abundance of oxygen defects, the 51% conversion of aniline catalyzed by NT-MnOOH-11 was 1.21 times higher than that (42%) catalyzed by NT-MnOOH-12. This comparison further revealed that more surface Mn^{3+} species provided more active sites for aniline adsorption, resulting in improved catalytic activity.

Despite the relatively lower amount of the surface Mn^{3+} species of NT-MnOOH-8 ($|\Delta AOS| = 0.067$) in comparison with NT-MnOOH-9 ($|\Delta AOS| = 0.048$), the NT-MnOOH-8 catalyst still delivered a much higher activity, which could be attributed to the significantly higher concentration of surface oxygen defects (Fig. 4a). Thus, it is reasonable that the surface oxygen defects also play a critical role in the catalytic activity. As shown in Fig. 4b, the catalytic activity of the five NT-MnOOH catalysts is presented as a function of surface oxygen defects, in which the higher level of surface oxygen defects associated with the enhanced mobility of lattice oxygen resulted in the higher conversion of aniline. Although NT-MnOOH-11 exhibited a similar level of surface oxygen defects in comparison with NT-MnOOH-12, the NT-MnOOH-12 catalyst delivered a much lower

This journal is © The Royal Society of Chemistry 2021

J. Mater. Chem. A, 2021, **9**, 19692–19697 | **19695**

Fig. 4 region
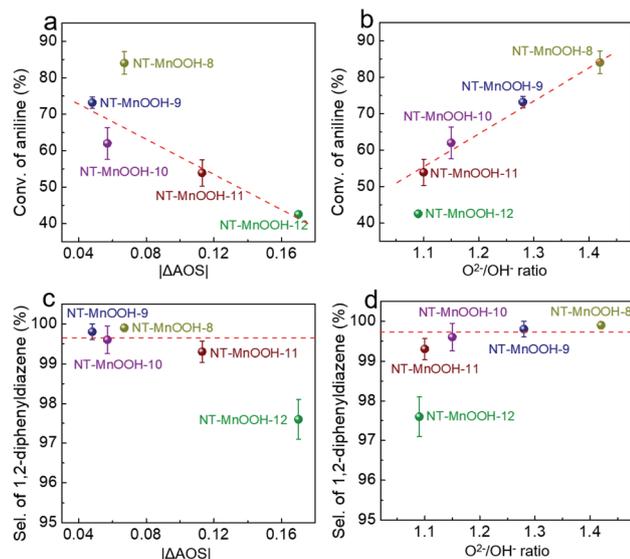
Fig. 4 The conversion of aniline as functions of (a) surface Mn³⁺ fraction and (b) surface oxygen defects. The selectivity of 1,2-diphenyldiazene as functions of the (c) surface Mn³⁺ fraction and (d) surface oxygen defects. Reaction conditions: aniline (0.5 mmol), catalysts (20 mg), toluene (2 mL), 0.5 MPa O₂, 60 °C and 8 h.

conversion of aniline, due to the decrease of the surface Mn^{3+} fraction. Therefore, both the surface Mn^{3+} species and oxygen defects contribute to the catalytic activity of NT-MnOOH, where the Mn^{3+} sites work as the active centre for the adsorption and activation of aniline and the surface oxygen defects benefit the mobility of lattice oxygen and oxidize aniline afterwards.

Fig. 4c and d exhibit the selectivity of 1,2-diphenyldiazene as functions of the surface Mn^{3+} level ($|\Delta AOS|$) and surface oxygen defect abundance (O^{2-}/OH$^-$ ratios). Both high levels of surface Mn^{3+} species and the large amount of surface oxygen defects facilitated the improvement of the selectivity of 1,2-diphenyldiazene. The NT-MnOOH-12 catalyst with the lowest surface Mn^{3+} level and the smallest amount of surface oxygen defects exhibited the lowest selectivity towards 1,2-diphenyldiazene. Comparatively, other NT-MnOOH-t catalysts yielded at least 99.3% selectivity (Fig. 4c and d). Among them, the NT-MnOOH-8 catalyst with the optimized surface properties delivered the best chemoselectivity towards azo compounds.

Scheme 1 The proposed catalytic process for oxidative coupling of anilines using NT-MnOOH.

Table 1 Oxidative coupling of various substituted anilines^a

Entry	Product	Time (h)	Conv. (%)	Sel. (%)
1		11	>92.9	>99.9
2		9	>99.9	98.5
3		10	94.2	98.7
4		8	>99.9	>99.9
5		24	>99.9	>99.9
6		24	97.3	>99.9
7		24	>99.9	>99.9
8		24	>99.9	>99.9

^{a} Reaction conditions: R-NH₂ (0.5 mmol), NT-MnOOH (20 mg), toluene (2 mL), 60 °C and 0.5 MPa O₂.

Based on the above analysis, the high level of surface Mn^{3+} species provides rich active sites for aniline adsorption (I) and subsequent activation along with Mn^{3+} to Mn^{2+} (II) and abundance of oxygen defects significantly contributes to the superior catalytic activity *via* the promoted mobility of lattice oxygen (III), as shown in Scheme 1. As a result, the NT-MnOOH-8 catalyst with the optimal surface properties exhibited the highest catalytic activity for oxidative coupling of aniline, leading to successful reaction even at room temperature. The high selectivity is mainly dependent on the richness of the surface Mn^{3+} sites. The high level of Mn^{3+} sites in NT-MnOOH induces a strong preferential adsorption of aniline and suppresses the adsorption of toluene on the catalyst surface, thus preventing the occurrence of the side reaction of toluene oxidation. Inspired by this model reaction, amines with various substituents were also successfully and selectively transformed into corresponding aromatic azo compounds using the NT-MnOOH catalyst at 60 °C and 0.5 MPa O₂ (Table 1).

Conclusions

The highly selective oxidative coupling of anilines to aromatic azo compounds has been successfully demonstrated with a mild reaction procedure using single crystal MnOOH nanotubes with abundant surface Mn^{3+} species and oxygen defects.

19696 | *J. Mater. Chem. A*, 2021, **9**, 19692–19697

This journal is © The Royal Society of Chemistry 2021

In this catalytic system, high selectivity is achieved with the usage of O_2 as the terminal oxidant at low temperatures in the absence of any other additives. The rich surface Mn^{3+} sites and abundant oxygen defects of NT-MnOOH induce strong aniline adsorption, promoting the formation of the corresponding radical cation to enhance the catalytic activity and suppressing the toluene oxidation to improve the catalytic selectivity. Such unique surface properties of MnOOH may also facilitate other oxidative reactions.

Author contributions

Z. S. and Q. Y. Q. conceived and directed the research. Z. Y. conducted the experiments of the catalyst preparation, selective oxidative coupling of anilines, and performed the experimental characterization. C. F. X. conducted FT-IR and H_2-TPR of catalysts. Z. M. K. and L. J. Y. checked the manuscript. The manuscript was written through contributions of all authors. All authors have given approval to the final version of the manuscript.

Conflicts of interest

There are no conflicts to declare.

Acknowledgements

Notes and references

1 A. Grirrane, A. Corma and H. García, *Science*, 2008, **322**, 1661–1664.
2 L. Liu, P. Concepción and A. Corma, *J. Catal.*, 2019, **369**, 312–323.
3 H. Yu, S. Han, Y. Cheng, S. Liu, C. Tao, A. Wang, W. Wei and Y. Wei, *Angew. Chem., Int. Ed.*, 2021, **60**, 6382–6385.
4 T. H. L. Nguyen, N. Gigant and D. Joseph, *ACS Catal.*, 2018, **8**, 1546–1579.
5 B. Mondal and P. S. Mukherjee, *J. Am. Chem. Soc.*, 2018, **140**, 12592–12601.
6 M. Barbero, S. Cadamuro, S. Dughera and C. Giaveno, *Eur. J. Org. Chem.*, 2006, **2006**, 4884–4890.
7 Z. Liu and M. Jiang, *J. Mater. Chem.*, 2007, **17**, 4249–4254.
8 Y. Takeda, S. Okumura and S. Minakata, *Angew. Chem., Int. Ed.*, 2012, **51**, 7804–7808.
9 A. Grirrane, A. Corma and H. Garcia, *Nat. Protoc.*, 2010, **5**, 429–438.
10 L. Hu, X. Cao, L. Chen, J. Zheng, J. Lu, X. Sun and H. Gu, *Chem. Commun.*, 2012, **48**, 3445–3447.
11 H. Zhu, X. Ke, X. Yang, S. Sarina and H. Liu, *Angew. Chem., Int. Ed.*, 2010, **49**, 9657–9661.
12 D. Combita, P. Concepción and A. Corma, *J. Catal.*, 2014, **311**, 339–349.
13 A. Noschese, A. Buonerba, P. Canton, S. Milione, C. Capacchione and A. Grassi, *J. Catal.*, 2016, **340**, 30–40.
14 S. Cai, H. Rong, X. Yu, X. Liu, D. Wang, W. He and Y. Li, *ACS Catal.*, 2013, **3**, 478–486.
15 X. Liu, H. Q. Li, S. Ye, Y. M. Liu, H. Y. He and Y. Cao, *Angew. Chem., Int. Ed.*, 2014, **53**, 7624–7628.
16 C. Zhang and N. Jiao, *Angew. Chem., Int. Ed.*, 2010, **49**, 6174–6177.
17 A. R. Patel, G. Patel, G. Maity, S. P. Patel, S. Bhattacharya, A. Putta and S. Banerjee, *ACS Omega*, 2020, **5**, 30416–30424.
18 S. S. Acharyya, S. Ghosh and R. Bal, *ACS Sustainable Chem. Eng.*, 2014, **2**, 584–589.
19 Y. Dai, C. Li, Y. Shen, T. Lim, J. Xu, Y. Li, H. Niemantsverdriet, F. Besenbacher, N. Lock and R. Su, *Nat. Commun.*, 2018, **9**, 60.
20 S. Biswas, K. Mullick, S. Y. Chen, D. A. Kriz, M. D. Shakil, C. H. Kuo, A. M. Angeles-Boza, A. R. Rossi and S. L. Suib, *ACS Catal.*, 2016, **6**, 5069–5080.
21 S. Sui, P. Zhang, H. Zhang and R. Cao, *Chin. J. Catal.*, 2019, **40**, 1525–1533.
22 Y. Cheng, T. Huang, Y. Sun and X. Shi, *Chem. Eng. J.*, 2017, **322**, 82–89.
23 P. Zhang, H. Lu, Y. Zhou, L. Zhang, Z. Wu, S. Yang, H. Shi, Q. Zhu, Y. Chen and S. Dai, *Nat. Commun.*, 2015, **6**, 8446.
24 S. Biswas, B. Dutta, K. Mullick, C. H. Kuo, A. S. Poyraz and S. L. Suib, *ACS Catal.*, 2015, **5**, 4394–4403.
25 B. Dutta, S. Biswas, V. Sharma, N. O. Savage, S. P. Alpay and S. L. Suib, *Angew. Chem., Int. Ed.*, 2016, **55**, 2171–2175.
26 S. Liu, Z. R. Tang, Y. Sun, J. C. Colmenares and Y. J. Xu, *Chem. Soc. Rev.*, 2015, **44**, 5053–5075.
27 Z. R. Tang, B. Han, C. Han and Y. J. Xu, *J. Mater. Chem. A*, 2017, **5**, 2387–2410.
28 S. Liu, C. Han, Z. R. Tang and Y. J. Xu, *Mater. Horiz.*, 2016, **3**, 270–282.
29 D. Huo, M. J. Kim, Z. Lyu, Y. Shi, B. J. Wiley and Y. Xia, *Chem. Rev.*, 2019, **119**, 8972–9073.
30 S. Zhang, Z. Q. Huang, Y. Ma, W. Gao, J. Li, F. Cao, L. Li, C. R. Chang and Y. Qu, *Nat. Commun.*, 2017, **8**, 15266.
31 S. Zhang, Z. Xia, Y. Zou, F. Cao, Y. Liu, Y. Ma and Y. Qu, *J. Am. Chem. Soc.*, 2019, **141**, 11353–11357.
32 A. S. Poyraz, J. Laughlin and Z. Zec, *Electrochim. Acta*, 2019, **305**, 423–432.
33 A. Longo, L. F. Liotta, G. D. Carlo, F. Giannici, A. M. Venezia and A. Martorana, *Chem. Mater.*, 2010, **22**, 3952–3960.
34 W. Yang, Y. Peng, Y. Wang, Y. Wang, H. Liu, Z. a. Su, W. Yang, J. Chen, W. Si and J. Li, *Appl. Catal., B*, 2020, **278**, 119279.
35 Y. Huang, M. Luo, S. Li, D. Xia, Z. Tang, S. Hu, S. Ye, M. Sun, C. He and D. Shu, *J. Hazard. Mater.*, 2021, **410**, 124545.